Hot-Electron Transfer Hot Paper

DOI: 10.1002/anie.201405598

Hot-Electron-Transfer Enhancement for the Efficient Energy Conversion of Visible Light**

*Sungju Yu, Yong Hwa Kim, Su Young Lee, Hyeon Don Song, and Jongheop Yi**

Abstract: *Great strides have been made in enhancing solar energy conversion by utilizing plasmonic nanostructures in semiconductors. However, current generation with plasmonic nanostructures is still somewhat inefficient owing to the ultrafast decay of plasmon-induced hot electrons. It is now shown that the ultrafast decay of hot electrons across Au nanoparticles can be significantly reduced by strong coupling with CdS quantum dots and by a Schottky junction with perovskite $SrTiO_3$ nanoparticles. The designed plasmonic nanostructure with three distinct components enables a hot-electron-assisted energy cascade for electron transfer, CdS→Au→$SrTiO_3$, as demonstrated by steady-state and time-resolved photoluminescence spectroscopy. Consequently, hot-electron transfer enabled the efficient production of H_2 from water as well as significant electron harvesting under irradiation with visible light of various wavelengths. These findings provide a new approach for overcoming the low efficiency that is typically associated with plasmonic nanostructures.*

Plasmonic nanostructures have recently been proposed to enhance the efficiency of solar energy conversion.[1] One of the remarkable features of plasmon-induced photocatalysis is localized surface plasmon resonance (LSPR), which arises from the collective oscillation of free electrons at the metallic interface or in small metallic nanostructures.[2] The phenomenon confers several distinct advantages to photocatalytic processes. First, plasmonic metal nanoparticles (NPs) act as photosensitizers in metal/semiconductor junctions and strongly absorb at specific wavelengths in the visible region. Second, the metallic NPs effectively act as antennae, which are useful in semiconductors with a short minority carrier diffusion length. The results of femtosecond pump–probe experiments suggest that the hot electrons in Au NPs have an elastic mean free path of approximately 10 nm.[3] However, hot-electron transfer to an adjacent semiconductor still remains a challenge because the hot electrons decay rapidly to lower energy levels through ultrafast electron–electron and electron–phonon scattering on a time scale of a few to several hundred femtoseconds.[4] The first demonstration of a plasmon-induced hot-electron transfer process in metal–semiconductor nanostructures by Wu et al. revealed that the plasmon excitation of Au led to the injection of hot electrons into the conduction band (CB) of CdS with an average quantum yield of approximately 2.75(±0.07)%.[4a] The low quantum yield was found to be the result of multiple competing pathways for energy dissipation in the hot electron injection process.

Herein, a combinative NP system composed of $SrTiO_3$ as a high-performance electron filter and a Au@CdS core–shell NP as the plasmonic photosensitizer was found to enhance hot-electron transfer. The ultrafast decay of the resulting hot electrons was efficiently reduced by the strong coupling of Au and CdS. Furthermore, a Schottky junction between Au and $SrTiO_3$ facilitated the charge transfer to the CB of $SrTiO_3$, and in turn, perovskite $SrTiO_3$ enabled the favorable transfer of charge carriers to active sites for H_2 production. Our findings also indicate the existence of a favorable electron pathway, CdS→Au→$SrTiO_3$, as shown by steady-state and time-resolved photoluminescence spectroscopy. This novel plasmonic nanostructure provides a new and effective strategy for the efficient energy conversion of visible light.

The synthesis of a Au@CdS core–shell NP deposited on the surface of a $SrTiO_3$ NP (Au@CdS/$SrTiO_3$) is schematically shown in Figure 1a. The detailed experimental procedures are given in the Supporting Information. In short, the positively charged surface of $SrTiO_3$ assists in the adsorption of $AuCl_4^-$ anions in a pH-controlled environment. Au NPs are deposited on the $SrTiO_3$ surface using $NaBH_4$, a strong reducing agent. Au@CdS core–shell structures are formed in an ethanol suspension containing Au/$SrTiO_3$, sulfur, and Cd^{2+} cations. Excess sulfur molecules with an affinity for Au are adsorbed on the surface of the Au NPs. When the resulting suspension is irradiated with UV light, the sulfur molecules that are adsorbed on the Au NPs are reduced to S^{2-} anions, which instantly react with Cd^{2+} cations to form CdS shells around the Au NPs. Although the Au@CdS core–shell structure has been proposed by our group and by Tada et al. for a solid-state Z-scheme under visible-light or UV irradiation,[5] the preparation method described in this study was altered so as to optimize the response of the Au NPs to visible-light irradiation by the LSPR effect. For example, the method resulted in Au NPs with a controlled size and the deposited Pt NPs functioned as a co-catalyst on the surface of

[*] S. Yu, Y. H. Kim, S. Y. Lee, H. D. Song, Prof. J. Yi
World Class University Program of Chemical Convergence for Energy & Environment, School of Chemical and Biological Engineering, Institute of Chemical Processes
Seoul National University
Seoul 151-742 (Republic of Korea)
E-mail: jyi@snu.ac.kr
Homepage: http://empl.snu.ac.kr

[**] This research was supported by the Global Frontier R&D Program of the Center for Multiscale Energy System of the National Research Foundation funded by the Ministry of Science, ICT & Future, Korea (NRF-2011-0031571). We thank the Supercomputing Center Korea of the Institute of Science and Technology Information for providing supercomputing resources and technical support (KSC-2013-C1-023).

Supporting information for this article is available on the WWW under http://dx.doi.org/10.1002/anie.201405598.

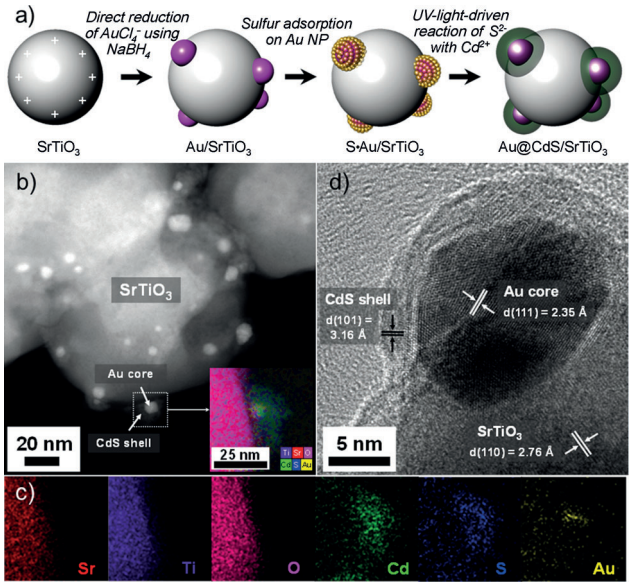

Figure 1. Morphology and composition of the $Au@CdS/SrTiO_3$ nanostructures as determined using microscopy techniques. a) Preparation of the $Au@CdS/SrTiO_3$ nanostructures. The first image (left) indicates the surface state of a $SrTiO_3$ NP with positive charges in an aqueous suspension at pH 4. The second image illustrates the deposition of Au NPs on the surface of $SrTiO_3$ by direct reduction of $AuCl_4^-$ using $NaBH_4$. Third, sulfur molecules are adsorbed onto the surface of the Au NPs because of their affinity to Au. Finally, the sulfur molecules are reduced to S^{2-} ions, which instantly react with Cd^{2+} to form CdS shells under UV irradiation. b) HAADF-STEM image of the Au@CdS core–shell structures distributed on the surface of a $SrTiO_3$ NP. c) 2D atomic mapping of Sr, Ti, O, Cd, S, and Au obtained by analytical STEM-EDS. d) HR-TEM image of the interface region of $SrTiO_3$ and Au@CdS.

the $SrTiO_3$. Furthermore, the $Au@CdS/SrTiO_3$ nanostructure entirely reversed the Z-schematic charge-transfer direction and even changed the main active site for H_2 generation from CdS to $SrTiO_3$. Notably, whereas two semiconductors that consist of the Z-schematic system should generate electron–hole pairs, $SrTiO_3$ NPs in the $Au@CdS/SrTiO_3$ nanostructure do not generate electrons during the H_2 generation but act as an electron filter for efficient hot-electron transfer.

The high-angle annular dark-field scanning transmission electron microscopy (HAADF-STEM) image in Figure 1b shows that the as-synthesized $Au@CdS/SrTiO_3$ NPs contain a few Au cores with a diameter of 11.5 ± 4.7 nm (see Figure S1a–e), which are deposited on the surface of the $SrTiO_3$ NPs (< 100 nm); CdS shells with a thickness of 3–5 nm are formed around the Au cores. Figure 1c displays the energy-dispersive X-ray spectroscopy (EDS) results of the core–shell structure marked in Figure 1b, which confirmed that the material is composed of a Au core with a CdS shell deposited on the surface of a $SrTiO_3$ NP. The high-resolution transmission electron microscopy (HR-TEM) image shown in Figure 1d was taken at the interface region of the $SrTiO_3$ and the Au@CdS core–shell NP and clearly reveals three distinct types of lattice fringes, which were assigned to $SrTiO_3$ (JCPDS 01-1018), Au (JCPDS 01-1172), and CdS (JCPDS 41-1049). The interface between the $SrTiO_3$ and Au core is believed to be important for the injection of hot electrons from Au to the CB of $SrTiO_3$ upon LSPR excitation.

Photocatalytic H_2 production was performed under irradiation with visible light ($\lambda \geq 400$ nm) in an aqueous suspension (Figure 2). The photocatalytic activities of bare $SrTiO_3$, $Au/SrTiO_3$, $CdS/SrTiO_3$, and $Au/CdS/SrTiO_3$ were compared with that of $Au@CdS/SrTiO_3$ by using samples that had almost

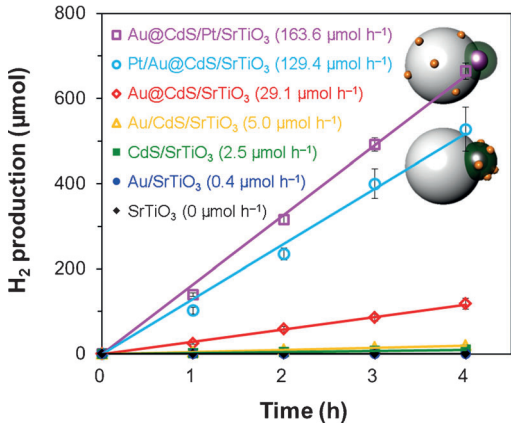

Figure 2. Photocatalytic H_2 production as a function of time under visible-light irradiation ($\lambda \geq 400$ nm).

the same Au (1 wt%) and CdS (4 wt%) concentrations, as determined by inductively coupled plasma atomic emission spectroscopy (ICP-AES). The H_2 production of bare $SrTiO_3$ is negligible because the catalyst can only be excited by UV light. Approximately 0.4 μmol h^{-1} (quantum efficiency, QE = 0.03%) H_2 molecules were produced by the $Au/SrTiO_3$ catalyst, despite the poor sensitivity of $SrTiO_3$ to visible light. The performance of $Au/SrTiO_3$ can be attributed to the injection of plasmon-induced hot electrons into the CB of $SrTiO_3$. $CdS/SrTiO_3$ produced H_2 at a rate of 2.5 μmol h^{-1} (QE = 0.19%). It is well-known that CdS-sensitized semiconductor composites (e.g., CdS/TiO_2) can generate large amounts of H_2 because of the enhanced charge separation that is due to the heterojunction structure.[6] Parts of the Au NPs that are not covered with CdS can act as a co-catalyst for H_2 production. A $Au/CdS/SrTiO_3$ photocatalyst for which Au and CdS NPs were individually deposited on the surface of $SrTiO_3$, was examined for the sake of comparison. The photocatalyst produced H_2 at a rate of 5.0 μmol h^{-1} (QE = 0.38%), which was twice as fast as the rate determined for $CdS/SrTiO_3$. This is due to the fact that the photoexcited electrons in the CB of CdS are shuttled to the CB of $SrTiO_3$, and are then entrapped by Au NPs, which accelerates H_2 production. Interestingly, $Au@CdS/SrTiO_3$ showed an impressive photosynthetic H_2 production rate of 29.1 μmol h^{-1} (QE = 2.21%). This can be attributed to the synergistic effects of 1) the plasmonic photosensitization of the Au@CdS core–shell structure, 2) the formation of a Schottky junction between the Au core and $SrTiO_3$, and 3) the high CB of perovskite $SrTiO_3$ with respect to the water-reduction potential. The efficient H_2 production with $Au@CdS/SrTiO_3$ is

explained in detail in the Supporting Information (see the Section on synergistic effects, Figure S2–3).

To investigate the electron-transfer processes, we prepared control samples of Pt/Au@CdS/$SrTiO_3$ and Au@CdS/Pt/$SrTiO_3$ nanocomposites. For the Pt/Au@CdS/$SrTiO_3$ photocatalyst, Pt NPs (1 wt%) were deposited on the CdS shell by the Z-scheme mechanism for Au@CdS/$SrTiO_3$ under irradiation with UV light (Figure S4 a–c). For the synthesis of Au@CdS/Pt/$SrTiO_3$, Pt NPs (1 wt%) were deposited on the surface of the $SrTiO_3$ by the direct reduction method using $NaBH_4$ before the formation of Au@CdS core–shell structures on the $SrTiO_3$ surface (Figure S5 a, b). Using Pt/Au@CdS/$SrTiO_3$ and Au@CdS/Pt/$SrTiO_3$, H_2 was produced at a rate of 129.4 (QE = 9.81%) and 163.6 μmol h^{-1} (QE = 12.41%), respectively. The experimental results imply that most of the photoexcited electrons that originate from the Au@CdS core–shell structures flow to the surface of the $SrTiO_3$ NP through a cascade of energy states. To further demonstrate the hot-electron-assisted charge dynamics of Au@CdS/$SrTiO_3$, we carried out steady-state and time-resolved photoluminescence (PL) measurements. The details of the steady-state PL spectra are provided in the Supporting Information (see the Section on electron-transfer dynamics, Figure S6 a–c), where the electron-transfer processes that determine the kinetics of the target system are also explained. Figure 3 a and b show the time-resolved PL spectra of the prepared samples suspended in an aqueous solution of rhodamine B (RhB, indicator dye to monitor interfacial charge transfer) with excitation wavelengths of 405 nm (for the excitation of CdS) and 500 nm (for the simultaneous excitation of CdS and Au). The resulting fluorescence was analyzed and fitted to a multi-exponential model. In the model equation, the intensity is assumed to decay as a sum of individual single exponential decays and described as:

$$I(t) = \sum_{i=1}^{n} A_i e^{-t/\tau_i} \quad (1)$$

where τ_i is the decay time, A_i represents the amplitude of the components at $t = 0$, and n is the number of decay times. The quality of the fitting was assessed by the reduced χ^2 value. All of the fitting parameters are summarized in Tables S1 and S2. The fluorescence decays of RhB and of RhB in the presence of CdS can be expressed as single-exponential functions, as CdS hardly emits PL at the excitation wavelength. However, the decay traces of RhB in the presence of $SrTiO_3$, Au/$SrTiO_3$, CdS/$SrTiO_3$, and Au@CdS/$SrTiO_3$ are expressed as bi-exponential functions as both RhB and $SrTiO_3$ emit PL at 580 nm. The obtained time-resolved spectra represent the sum of PL_1 of RhB and PL_2 of $SrTiO_3$. Therefore, the pre-exponential factors A_i indicate the relative contribution of PL_1 and PL_2 to the time-resolved PL spectra. τ_1 and τ_2 in the exponential term describe the decay of the electron population in photoexcited RhB and in the CB of $SrTiO_3$, respectively. The decay rates of the electron populations in RhB and in the CB of $SrTiO_3$ could be experimentally assessed by fitting the time-resolved PL curve to Eq. (1). In an attempt to understand the kinetics of the process based on the results of the steady-state PL spectroscopy data, electron pathways were constructed with differential equations (see Table S3 and S4). In the schematic representation, R, S, A, and C denote RhB, $SrTiO_3$, Au, and CdS, respectively. Furthermore, $N_R(t)$ and $N_S(t)$ refer to the time-dependent electron populations of the lowest unoccupied molecular orbital (LUMO) of RhB and the CB of $SrTiO_3$, respectively. The rate constants were calculated by comparing the exponents, k, in the differential equations with the values for τ_i that were extracted from the fitted results of the time-resolved PL spectra. Table S5 summarizes the electron-transfer rate constants at the different excitation wavelengths. The fluorescence of pure RhB at the excitation wavelength ($\lambda_{ex} = 405$ nm) showed a single-exponential decay with an emission lifetime of 1.711 ns, which was constant at the long excitation wavelength ($\lambda_{ex} = 500$ nm), and its recombination rate constant based on the expression $k_R = 1/\tau_1(\text{RhB})$ was approximately 5.84×10^8 s^{-1}. The addition of $SrTiO_3$ led to faster fluorescence decay of RhB, which could be described by the bi-exponential model. The interfacial charge transfer from the excited RhB to the CB of $SrTiO_3$ decreased the

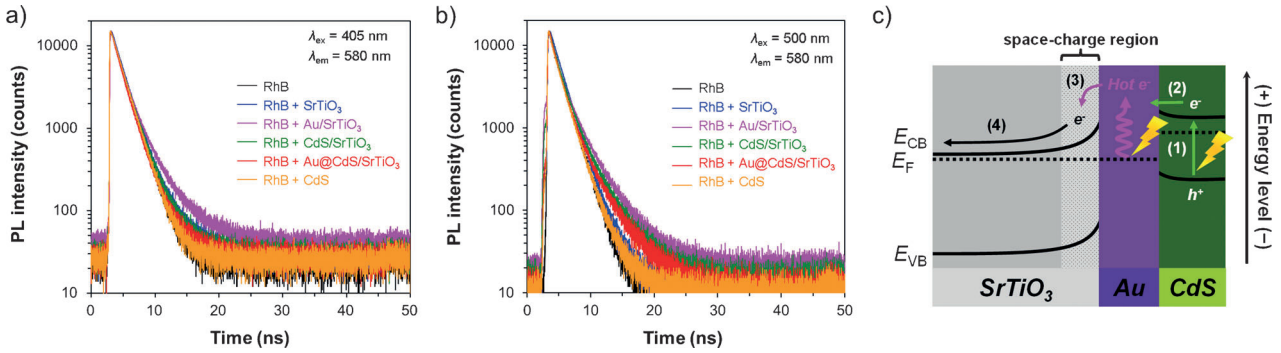

Figure 3. Time-resolved PL spectra of a RhB solution (1 μM) in the presence of the indicated sample with a) excitation at 405 nm and b) excitation at 500 nm, where the emission wavelength is 580 nm. c) Schematic energy band diagram of Au@CdS/$SrTiO_3$, showing the proposed electron-transfer processes across the three components responsible for H_2 production. The numbered arrows indicate the following individual electron-transfer steps: 1) Excitation of electrons in the CdS shell, 2) electron injection from the CB of the CdS shell into the Fermi level of the Au core, 3) plasmon-induced hot electron injection from the Au core into the CB of $SrTiO_3$, and 4) migration of the hot electrons to active sites at the surface of $SrTiO_3$.

lifetime, τ_1, of RhB. Its rate constants for the charge transfer, $k_{R\rightarrow S}$, were $0.38\times10^8\ s^{-1}$ at $\lambda_{ex}=405$ nm and $0.32\times10^8\ s^{-1}$ at $\lambda_{ex}=500$ nm. Furthermore, the recombination rate constants for $SrTiO_3$ could be obtained from the second lifetime, τ_2, which was affected by the fluorescence decay of $SrTiO_3$. The corresponding rate constants, k_S, were determined to be $2.80\times10^8\ s^{-1}$ at $\lambda_{ex}=405$ nm and $2.90\times10^8\ s^{-1}$ at $\lambda_{ex}=500$ nm. Au/$SrTiO_3$ NPs suspended in RhB facilitated the fluorescence decay of RhB, as the photoexcited electrons from RhB were further transferred to the Fermi level of the Au NPs at a rate, $k_{R\rightarrow A}$, of approximately $0.42\times10^8\ s^{-1}$ at $\lambda_{ex}=405$ nm. The rate increased to $1.17\times10^8\ s^{-1}$ for an excitation wavelength of 500 nm. The increase can be attributed to the LSPR excitation of the Au NPs, leading to hot-electron transfer to the CB of $SrTiO_3$. As Au and CdS did not emit PL, most of the electrons injected into the Au or CdS particles from RhB were assumed to be transferred to the CB of $SrTiO_3$. Therefore, we designated $k_{R\rightarrow A}$ to be $k_{R\rightarrow A\rightarrow S}$ at $\lambda_{ex}=500$ nm. However, the deposition of Au NPs caused the electrons in the CB of $SrTiO_3$ to recombine at the Fermi level of Au. The rate constant for this process, $k_{S\rightarrow A}$, was $0.04\times10^8\ s^{-1}$ at $\lambda_{ex}=405$ nm and $0.10\times10^8\ s^{-1}$ at $\lambda_{ex}=500$ nm. CdS/$SrTiO_3$ NPs suspended in RhB also promoted the fluorescence decay of RhB as the photoexcited electrons from RhB are sequentially transferred to the CB of CdS and $SrTiO_3$ at a rate $k_{R\rightarrow C\rightarrow S}$. The rate constant $k_{R\rightarrow C\rightarrow S}$ ($0.85\times10^8\ s^{-1}$) at $\lambda_{ex}=500$ nm was lower than that ($1.01\times10^8\ s^{-1}$) at $\lambda_{ex}=405$ nm owing to the weak excitation of CdS, and the decay of electrons in the CB of $SrTiO_3$ to the VB of CdS, $k_{S\rightarrow C}$, occurred at a rate of $1.28\times10^8\ s^{-1}$ at $\lambda_{ex}=405$ nm and at $0.04\times10^8\ s^{-1}$ at $\lambda_{ex}=500$ nm. When the Au@CdS/$SrTiO_3$ NPs were suspended in RhB, the photoexcited electrons of RhB could be transferred to the CB of $SrTiO_3$ and the CdS shell. The electrons in the CB of the CdS shell could be injected into the Au core, which is strongly coupled to the CdS shell (see the Section on optical characterization in the Supporting Information, Figures S7 and S8). Then, the electrons that have been injected into the Au core are likely to decay to the VB of CdS at $\lambda_{ex}=405$ nm with a rate constant $k_{R\rightarrow C\rightarrow A\rightarrow C}$ ($1.10\times10^8\ s^{-1}$) or quench the remaining positive charges at the Au core upon LSPR excitation at $\lambda_{ex}=500$ nm. At $\lambda_{ex}=500$ nm, the separated hot electrons of the Au core could be sequentially transferred to the CB of $SrTiO_3$, and the rate constant for this process was denoted as $k_{R\rightarrow C\rightarrow A\rightarrow S}$. This rate constant ($1.94\times10^8\ s^{-1}$) was even higher than the $k_{R\rightarrow A\rightarrow S}$ ($1.17\times10^8\ s^{-1}$) rate constant of Au/$SrTiO_3$ at $\lambda_{ex}=500$ nm. These observations explain the enhancement of hot-electron transfer with Au@CdS/$SrTiO_3$.

Regarding the above results, we propose that the following electron-transfer processes occur in Au@CdS/$SrTiO_3$ NPs under visible-light irradiation (Figure 3c). The excitation of LSPR in the Au core transiently produces electron–hole pairs with hot electrons at empty states above the Fermi level of the Au core. When a certain number of hot electrons arrive at the interface of the Au core and $SrTiO_3$, a fraction of the hot electrons is injected into the CB of $SrTiO_3$.[7] The hot electrons then diffuse to the surface of the $SrTiO_3$ and are subsequently entrapped by Pt NPs, which provide active sites for H_2 production and enhance the charge separation. Meanwhile, a significant fraction of residual holes at the Au core are removed by the electrons injected from the CdS shell, and the sacrificial ions quench the holes in the CdS shell.

The previous sections focused on the conversion of visible light into chemical energy, H_2. Photoexcited electrons in the Au@CdS/$SrTiO_3$ nanostructure can also be used to directly generate electrical energy in a photoelectrochemical (PEC) cell. The details of this process are given in the Supporting Information (see the Section on photoelectrochemical performance characterization, Figure S9–S11).

In summary, we have demonstrated an enhancement in the hot-electron transfer of a Au core by strong electronic coupling to a CdS shell that is in direct contact with perovskite $SrTiO_3$ NPs for the effective conversion of visible light into clean H_2 or into electricity. The enhanced H_2 production can mainly be attributed to the synergistic effects of the following three features: 1) The plasmonic photosensitization of the Au@CdS core–shell NPs generates more active electron–hole pairs. 2) Band bending between the Au core and $SrTiO_3$ enables hot electrons to be easily ejected from the Au core into the CB of $SrTiO_3$. 3) Perovskite $SrTiO_3$ plays an important role as a high-performance electron filter that is superior to TiO_2, and has a sufficiently high CB to produce H_2. Consequently, the Au@CdS/$SrTiO_3$ nanostructure provided a favorable electron pathway, CdS→Au→$SrTiO_3$, for the efficient separation of electron–hole pairs, although Au, which displays a large work function, was sandwiched in between $SrTiO_3$ and CdS. The designed nanostructure achieved a remarkably efficient photocatalytic H_2 production and electron harvesting at various visible-light wavelengths. The findings from this study will be informative for the design of plasmonic photocatalysts and PEC cells, such as photovoltaic and water-splitting devices.

Received: May 24, 2014
Published online: August 28, 2014

Keywords: kinetics · nanomaterials · photocatalysis · solar energy conversion · surface plasmon resonance

[1] a) Y.-G. Lin, Y.-K. Hsu, Y.-C. Chen, S.-B. Wang, J. T. Miller, L.-C. Chen, K.-H. Chen, *Energy Environ. Sci.* **2012**, *5*, 8917 – 8922; b) Z. Liu, W. Hou, P. Pavaskar, M. Aykol, S. B. Cronin, *Nano Lett.* **2011**, *11*, 1111 – 1116; c) Y. Tian, T. Tatsuma, *J. Am. Chem. Soc.* **2005**, *127*, 7632 – 7637; d) J. Lee, S. Mubeen, X. Ji, G. D. Stucky, M. Moskovits, *Nano Lett.* **2012**, *12*, 5014 – 5019; e) S. Mubeen, J. Lee, N. Singh, S. Krämer, G. D. Stucky, M. Moskovits, *Nat. Nanotechnol.* **2013**, *8*, 247 – 251.

[2] a) X. Zhang, Y. L. Chen, R.-S. Liu, D. P. Tsai, *Rep. Prog. Phys.* **2013**, *76*, 046401 – 046443; b) S. C. Warren, E. Thimsen, *Energy Environ. Sci.* **2012**, *5*, 5133 – 5146; c) S. A. Maier in *Plasmonics: Fundamentals and Applications*, Spinger, New York, **2007**.

[3] a) J. Hohlfeld, S.-S. Wellershoff, J. Güdde, U. Conrad, V. Jähnke, E. Matthias, *Chem. Phys.* **2000**, *251*, 237 – 258; b) H. Inouye, K. Tanaka, *Phys. Rev. B* **1998**, *57*, 11334 – 11340.

[4] a) K. Wu, W. E. Rodríguez-Córdoba, Y. Yang, T. Lian, *Nano Lett.* **2013**, *13*, 5255 – 5263; b) J. H. Hodak, I. Martini, G. V. Hartland, *J. Phys. Chem. B* **1998**, *102*, 6958 – 6967.

[5] a) H. J. Yun, H. Lee, N. D. Kim, D. M. Lee, S. Yu, J. Yi, *ACS Nano* **2011**, *5*, 4084 – 4090; b) H. Tada, T. Mitsui, T. Kiyonaga, T. Akita, K. Tanaka, *Nat. Mater.* **2006**, *5*, 782 – 786.

[6] a) V. M. Daskalaki, M. Antoniadou, G. L. Puma, D. I. Kondarides, P. Lianos, *Environ. Sci. Technol.* **2010**, *44*, 7200 – 7205; b) J. S. Jang, H. G. Kim, P. H. Borse, J. S. Lee, *Int. J. Hydrogen Energy* **2007**, *32*, 4786 – 4791; c) H. Fujii, M. Ohtaki, K. Eguchi, H. Arai, *J. Mol. Catal. A* **1998**, *129*, 61 – 68; d) J. S. Jang, S. M. Ji, S. W. Bae, H. C. Son, J. S. Lee, *J. Photochem. Photobiol. A* **2007**, *188*, 112 – 119.

[7] a) M. W. Knight, H. Sobhani, P. Nordlander, N. J. Halas, *Science* **2011**, *332*, 702 – 704; b) Y. K. Lee, C. H. Jung, J. Park, H. Seo, G. A. Somorjai, J. Y. Park, *Nano Lett.* **2011**, *11*, 4251 – 4255; c) S. Mubeen, G. Hernandez-Sosa, D. Moses, J. Lee, M. Moskovits, *Nano Lett.* **2011**, *11*, 5548 – 5552.

